Acta Ciencia Indica, Vol. XLII P, No. 3, 139 (2016)

SYNTHESIS AND APPLICATIONS OF GRAPHENE

S. CHANDRA AND POOJA RANI

Department of Physics, Panjab University, Chandigarh-160014, India

RECEIVED : 22 August, 2016

REVISED : 31 August, 2016

In this paper we shown that although bulk graphite is a chemically inert material, the surface single layer graphene is rather reactive against individual atoms. So far a, synthesis of several graphene derivatives have been reported such as hydrogenated graphene "graphene" (CH), fluorographene (CF) and chlorographene (CCl). Moreover, the stability of bromine and iodine covered graphene were predicted using computational tools. Among the derivatives easy synthesis, insulating electronic behavior and reversibly tunable crystal structure of graphene make this material special for future ultra-thin device applications and the structural, electronic, magnetic, vibrational and mechanical properties of graphene are overview. We also efforts to the computational modeling of graphene and its derivatives. Furthermore recent progress in synthesis techniques and possible applications of graphene are reviewed as well.

KEYWORDS : Structure and Physical properties of graphene, Synthesis and Applications.

INTRODUCTION

During the last decade, the field of materials science has been expanded with the advent of few-atom-thick two-dimensional materials. Previously, the majority of research was devoted to three-dimensional bulk crystals because these are easier to handle in experiment and in theoretical simulations. The ever increasing trend to miniaturization in the last decades has been accompanied with the production of low-dimensional nanomaterials in all but two dimensions. The accepted theoretical impossibility of such 2D materials has probably been the largest obstacle for their fabrication. 2D systems, such as electron gases, have been known for quite some time, but they usually appear at the surface or interface of 3D materials. In material science, the dimensionality of a material is not a strictly defined quantity, but it is common to refer to few-atom-thick layers as 2D. In that sense, 2D materials have only come to the center of attention with the isolation and characterization of graphene in 2004 [1-4].

The production of graphene was originally achieved with the now famous scotch-tape method. Starting from a highly-ordered pyrolytic graphite sample, few-layer graphene samples are isolated by repeated peeling with an adhesive tape, and subsequent deposition on a substrate (usually silicon dioxide). Nowadays, many different techniques have been developed to produce graphene from other (3D) crystals such as silicon carbide or using bottom-up approaches.

Graphene is a unique material in many ways. It is the thinnest imaginable crystal but, at the same time, it is the strongest, stiffest, and best conducting material known [5-6]. Furthermore, it has an intriguing electronic spectrum that mimics that of massless Dirac particles, leading to many fascinating phenomena such as an anomalous integer quantum Hall effect and Klein tunneling. The absence of a band gap in the electronic spectrum of graphene can also be considered as an annoying feature that prohibits the direct implementation of graphene in electronics. Therefore, a large part of the research on graphene has been devoted to the creation of an electronic band gap. This can be achieved in many ways:

(i) through a reduction of the dimensionality by cutting graphene into ribbons or flakes,

(ii) by periodic potentials or substrates that break the sublattice symmetry, or

(iii) by the destruction of the π-bond network through functionalization.

Functionalization of graphene can be achieved in different ways. It is possible to substitute some C atoms in the graphene layer by foreign atoms such as B and N. In this way charge doping can be obtained and a small band gap can be opened. Another way of functionalization is through the adsorption of atoms or molecules. Depending on the adsorption strength, one can distinguish between physisorption and chemisorption. Physisorption leaves the graphene structure virtually unaltered, but can induce some subtle electronic changes such as charge doping. Chemisorption, on the other hand, is accompanied by strong covalent bonds between the graphene C atoms and the adsorbate. These covalent bonds disrupt the aromatic network in graphene and causes strong structural changes. The adsorbates that can cause these kind of changes are usually radicals such as hydroxyl groups or atomic species. When the coverage of chemisorbed adsorbates is dense enough, the properties of graphene can change drastically, as in the case of oxygenation [7-8]. A (reversible) metal to insulator transition is predicted upon covalent functionalization [9].

Table I. The relative stability of various graphane isomers with respect to the chair isomer as found in the literature. The total energies, calculated for per unit cell, are given in eV.

	Sluiter Ref.15	**Sofo Ref.16**	**Samarakoon Ref. 17**	**Leenaerts Ref. 18**	**Artyukhov Ref. 19**	**Wen Ref.20**	**Samarakoon Ref. 24**	**Bhattacharya Ref. 25**	**He Ref. 26**
Chair	0.000	0.00	0.00	0.000	0.000	0.00	0.00	0.00	0.000
Boat	0.103	0.12	0.17	0.103	0.103	0.10	0.09	0.10	0.102
Stirrup	0.056	-	-	0.053	0.055	0.05	0.05	0.04	0.056
Armchair	-	-	-	0.128	-	0.13	-	-	0.134
TB-chair	-	-	0.25	-	-	0.19	-	-	-
Twist-boat	-	-	-	-	-	-	0.16	-	0.150
Tricycle	-	-	-	-	-	-	-	-	0.024

Depending on the type of adsorbate the functionalized graphene can exhibit crystalline or amorphous character. The former is expected for hydrogenation and fluorination while the latter has been observed for oxygenated graphene (graphene oxide). The distinction between crystalline and amorphous is not always clear and can depend on the level of coverage. Furthermore it is expected that island formation occurs, which makes the distinction even more troublesome [10].

The chemical functionalization of graphitic materials has a longer experimental and theoretical history that dates back from before the isolation of graphene. Fluorinated graphite and fluorinated graphene have been thoroughly studied and much of the obtained knowledge can be transferred to the case of hydrogenated graphene [11-14].

METHODS

PROPERTIES OF GRAPHENE

Graphane is the name given to a class of hydrogenated graphene structures that are close to full coverage. Ideally, every carbon atom of the graphene layer is covalently bonded to a hydrogen atom. These C-H bonds can only exist if the C atoms in graphene change their hybridization from sp^2 to sp^3 and, as a consequence, the graphene layer becomes buckled. There is no unique way to couple every C to a H atom because the H atoms can attach to the graphene layer from above or below. In fact, there is also no a priori reason why this should be done in an ordered fashion, but to keep calculations and interpretations simple, one usually supposes the graphane structure to be crystalline. It is assumed that the H atoms are chemisorbed according to some simple pattern and during the last decade, many different patterns have been suggested. These are usually referred to as the different conformations, configurations, or (stereo) isomers of graphane. Note that the different CH structures are actually not conformers because they are not related by more bond rotations. In this para, we take a closer look at the structure and physical properties of the different graphane isomers. We review their electronic, vibrational, and optical properties and comment on their relative stability.

(i) Atomic Structure

In Fig. 1, we show the schematic structure of the three best-known and most stable graphane isomers, namely the chair, stirrup, and boat configuration, together with two other isomers.

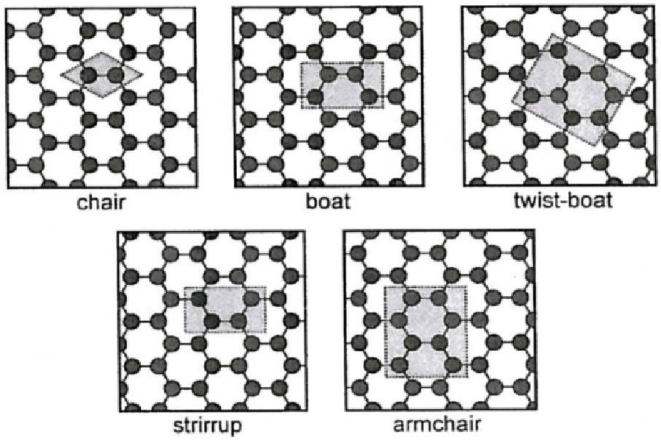

Fig. 1. Five isomers of graphane in which every C atom is equivalent. Blue and red colors indicate H adsorption, respectively, above and below the grapheme layer.

The former three structures have already been proposed in 2003, *i.e*. before the isolation of graphene, by Sluiter and Kawazoe [3, 15]. However, it took until 2007, when Sofo *et al*. rediscovered the chair and boat configurations, that graphane acquired widespread attention from the graphene community [16]. Since then, more structures have been proposed such as

the twist-boat, twist-boat-chair, armchair, tricycle, and many others, but they are all considerably less stable than the known configurations (except for the tricycle configuration which is actually a combination of chair and stirrup) and arc therefore of minor importance [24, 17, 18, 26]. In table I, we compare the calculated stability of different graphane configurations that can be found in the literature. All computational studies agree that the chair configuration is the most stable one. In this configuration the H atoms arc alternately adsorbed above and below the graphene sheet so that all the C atoms of one sublattice move up while those of the other sublattice move down Fig. 2 (a). Although less common in the literature, the stirrup configuration is also called washboard, or zigzag configuration, is more stable than the so called boat configuration.

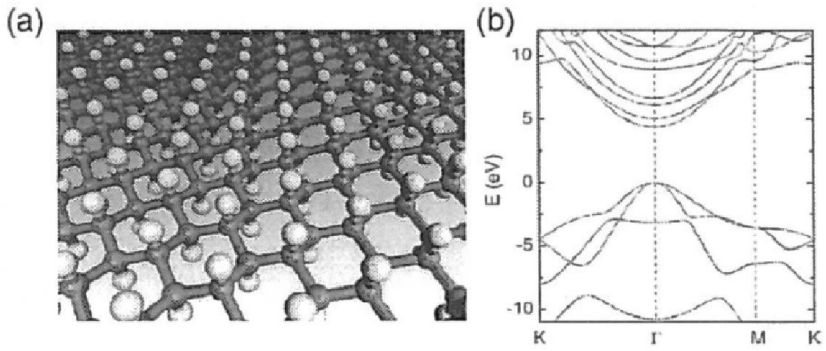

Fig. 2. (a) Crystal structure of graphane in chair configuration (b) Band structure of graphane.

The stirrup isomer, schematically shown at the bottom left of Fig. 1, consist of alternating zigzag chains with H atoms pointing up and down. The reason that this graphane isomer is less well-known is probably the fact that the important paper of Sofo *et al* [16] considered the boat configuration, but not the stirrup one.

In discussing the dependence of the properties on the type of conformation, we take the four isomers discussed by Leenaerts *et al* [18] as characteristic examples. Wen *et al*. showed that these isomers are dynamically more stable than benzene molecules [20]. The data for the structure of these graphane isomers are given in Table II.

Table II. Structure parameters for the different graphane isomers. Distances are given in Å and angles in degrees. The distance between neighboring C atoms, d_{cc}, and the angles, θ_{ccx}, are averaged over the supercell.

	Chair	**Boat**	**Strirrup**	**Armchair**
$a_x / \sqrt{3}$	2.539	2.480	2.203	2.483
a_y / n_y	2.539	2.520	2.540	2.270
d_{CH}	1.104	1.099	1.099	1.096
$\bar{d}_{cc}$	1.536	1.543	1.539	1.546
$\bar{\theta}_{CCH}$	107.4	107.0	106.8	106.7
$\bar{\theta}_{CCC}$	111.5	111.8	112.0	112.1

The length of the C-H bonds is about 1.10 Å which is typical for such bonds as found in organic chemistry. The average length of the C-C bonds is close to the ideal single C-C bonds in diamond. Since there is no steric strain in the chair configuration, because all bonds and angles arc completely free to relax, the bond lengths and angles can be considered ideal in that case. Deviations from this ideal situation are found in the other configurations which indicate the presence of local strain. Some of the isomers contain substantial structural anisotropies which are translated into their electronic and mechanical properties.

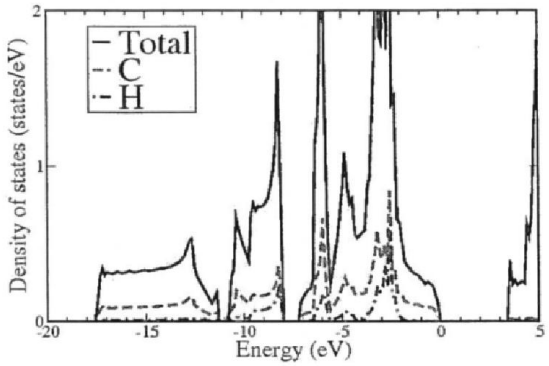

Fig. 3. The total and projected density of states of graphane.

(ii) Electronic Structure

Graphane is a semiconducting material with a substantial direct electronic band gap Fig. 2(b). The size of the gap depends on the method of calculation: within DFT the gap is about 3.5 eV for LDA and GGA, and 4.4 eV with a hybrid functional (HSE06) [22]. The hybrid functional (HSE) overcomes some deficiencies of the conventional approximations for the exchange-correlation (*xc*) functional within DFT, *i.e*. LDA or GGA [21-22]. The later include an unphysical interaction of the electron with itself, the so-called self-interaction, yielding a systematic underbinding of strongly localized states. HSE partly corrects for this spurious self-interaction by intermixing a fraction of Hartrec-Fock exchange. This leads to an improvement of the structural (equilibrium lattice constants, bulk moduli), thermochemical (cohesive energies, heats of formation), and electronic properties (bandgaps) of semiconductors and insulators [23]. Still higher accuracy on the electronic band gap can be achieved by including many-body interactions (GW approximation). Such many-body interactions increase the electronic band gap of graphane further to about 5.2 eV [18, 27].

The band gap is almost independent of the configuration and varies with less than 5% [18]. The total and projected density of states (DOS) of graphane in the chair configuration is shown in Fig. 3. The electronic gap is clearly recognizable in the total DOS, but the projected DOS shows some peculiar characteristics. The electronic states below the gap are localized on the C atoms but the contribution of C and H atoms to the conduction band states is negligible.

This is even more clear when considering the density of the single-particle states at the valence band maximum (VBM) and conduction band minimum (CBM), as shown in Fig. 4. The VBM and CBM have very different, character and symmetry. The valence band states consist of C_{px} and p_y orbitals, but the conduction band states exhibit plane-wave character. The CBM state behaves as a delocalized electron that is loosely bound above the H

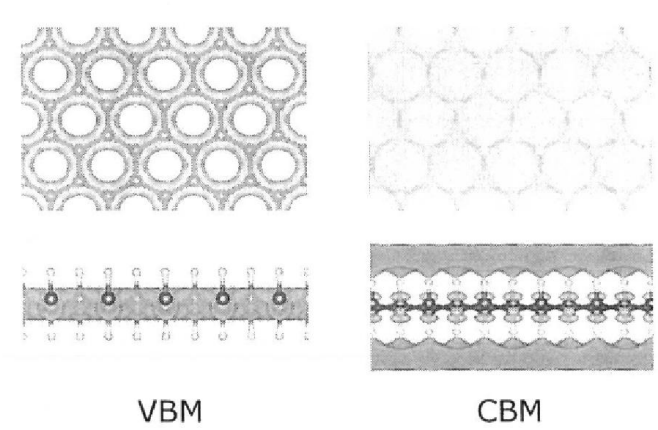

Fig. 4. Top and side views of the VBM (left) and CBM (right) states of graphane.

1. Optical Properties

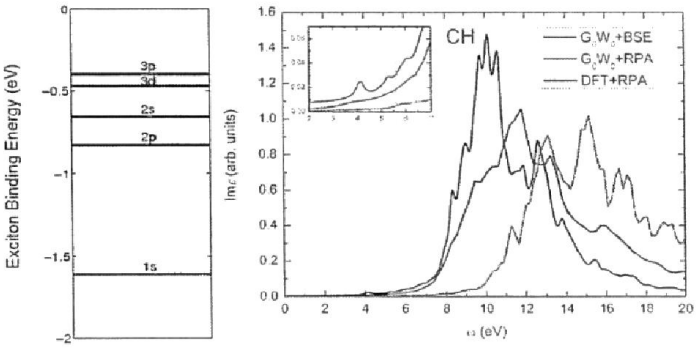

Fig. 5. The excitonic spectrum of bound states in grapheme in Color line (*L*). The imaginary part of the dielectric function of graphane calculated within DFT (DFT + RPA), with *e-e* interactions (G_0W_0 + RPA) and with *e-e* and *e-h* interaction (G_0W_0 + BSE) in (*R*).

The two-dimensional nature of graphane has a significant impact on its optical properties and reduces the optical band gap significantly. The reduced screening in two-dimensional materials leads to large electron-hole interaction [29]. As a consequence, there are bound exciton states considerably below the conduction band minimum. For graphane the exciton binding energy has been calculated to be 1.6 eV which produces an optical gap of about 3.8 eV [29-32]. A more complete exciton spectrum is shown in Fig. 5(L). The increase of the electronic band gap due to electron-electron interactions, is almost completely canceled by the electron-hole interaction. This is nicely illustrated in Fig. 5 (R) which shows the absorption spectra (imaginary part of the dielectric function) at 3 different levels of approximation : (i) without *e-e* and *e-h* interaction, (ii) with *e-e* but no *e-h* interaction, and (iii) with *e-e* and *e-h* interaction. Single-particle calculations (DFT) lead to similar band gaps as calculations with *e-e* and *e-h* interaction (G_0W_0 + BSE).

In experiments, one usually estimates the band gap from optical absorption measurements. This kind of measurements actually measures the optical band gap and not the electronic band gap. Therefore, one should take care to compare experimental results with the appropriate theoretical calculations.

2. Magnetic properties

Fully hydrogenated graphene contains only sp^3 hybridized C atoms with 4 bonding partners (3 C and 1 H).Therefore, the ideal graphane isomers are not expected to show any interesting magnetic properties. Magnetism only occurs at defect sites (missing H atoms) and in partially hydrogenated graphene [33-34]. We discuss this in more detail below. Substitutional defects such as B atoms, can also lead to a magnetic response in graphane [35].

Another important effect of hydrogenation of graphene is the enormous increase in spin-orbit coupling. The change in hybridization from sp^2 to sp^3 enhances the spin-orbit by two orders of magnitude. Atomic spin-orbit coupling in graphene is a very weak second order process, but, H adsorption can turn this into a first-order process. The spin-orbit coupling in graphene becomes of the order of the atomic spin-orbit coupling $(\Delta_{SO}^{at} \approx 10\,\text{meV})$ and is comparable to that of diamond.

3. Vibrational properties

In Fig. 6 the phonon spectrum of graphane in the chair configuration is shown. The absence of imaginary frequencies indicates that this graphane isomer is stable. The phonon modes of graphane can be divided into low, intermediate, and high-frequency groups of phonons [38]. From the projected phonon DOS, the high-frequency modes are identified as dominantly H modes, as can be expected from the CH stretching modes. The low-lying (acoustic) modes are dominantly C modes while the intermediate-frequency group of phonons have contributions from both types of atoms.

Savini *et al*. showed that upon hole doping, a giant Kohn anomaly arises in the intermediate-frequency (optical) phonon spectrum of graphane [39]. This phenomenon was predicted to turn graphane into an electron-phonon superconductor with a critical temperature above 90 K. This is a consequence of the unique strength of the chemical bonds between the carbon atoms and the large density of electronic states at the Fermi energy due to the reduced dimensionality of graphane.

In addition the presence and characteristic properties of discrete breathers (DBs) which are spatially localized,

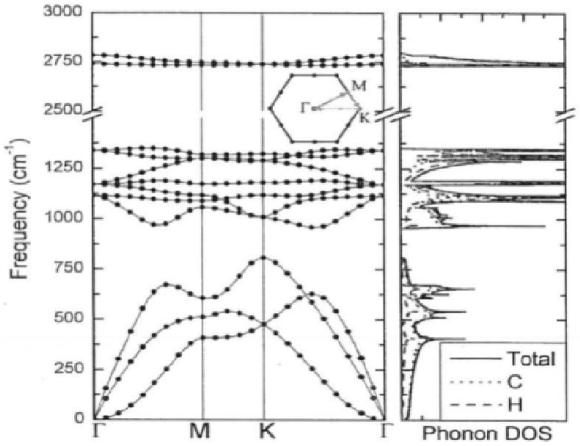

Fig. 6. Phonon dispersion of graphane in the chair configuration. The dots are the directly calculated frequencies and the lines are interpolated values. The inset shows the first Brillouin zone and the wave vector path used. The right-hand side shows the phonon DOS.

Large-amplitude vibrational modes in defect-free nonlinear lattices was investigated by Chechin *et al*. It is found that DB frequency decreases with increase in its amplitude, and it can take any value within the phonon gap and can even enter the low-frequency phonon band.

4. Mechanical properties

Graphene is the strongest material ever measured and it has also a remarkable stiffness. Hydrogenation reduces the strength of graphene because the strong aromatic bond network is replaced with single σ bonds. The 2D Young's modulus of graphane has been calculated to be around 245 Nm^{-1} which is substantially smaller than the calculated and experimental value for graphene 340 Nm^{-1} [5, 18, 41-43]. Experimental values for the Young's modulus of graphane are not available at present, but they are expected to be lower than the theoretical value due to the presence of defects.This is comparable to the case of fluorinated graphene where the theoretical estimate is about twice the experimental value [18, 44]. Other isomers of graphane such as the boat and stirrup configurations exhibit highly anisotropic behavior, The Young's modulus can decrease to half its value in particular directions and also the Poisson ratios are very anisotropic [45].

Perfect graphane behaves elastically under strains up to at least 30%, but small defects can drastically re-duce this limit. For larger strains, graphane shows irreversible changes and defects start to appear. The out-of-plane stifness of graphane is also somewhat smaller than that of graphene, leading to a higher surface roughness

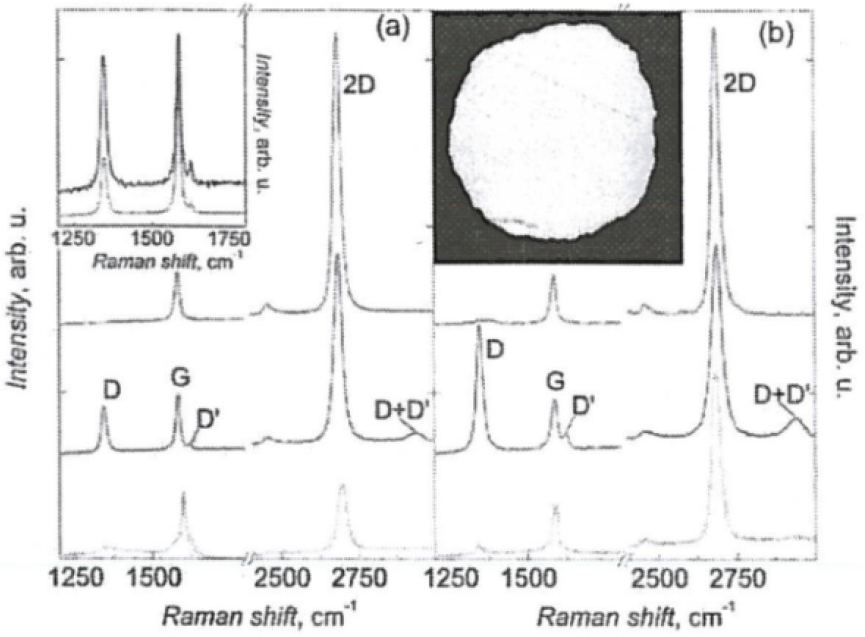

Fig. 7. Changes in Raman spectra of graphene caused by hydrogenation in Color line. The spectra are normalized to have a similar intensity of the G peak. (a) Graphene on SiO_2. (b) Free-standing graphene. Red, blue, and green curves (top to bottom) correspond to pristine, hydrogenated, and annealed samples, respectively. Reproduced with permission from The American Association for the Advancement of Science and thermal contraction under copy right 2009 [46].

Thermal fluctuations of single layer graphane were investigated by Costamagna *et al*. up to temperatures of at least 900 K [47]. By analyzing the mean square value of the height fluctuations and the height-height, correlation function for different system sizes and

temperatures, they showed that graphane was an unrippled system in contrast to graphene where later follows the membrane theory. This unexpected behavior persists and is a consequence of the fact that in graphane the thermal energy can be accommodated by in-plane bending modes, *i.e*., modes involving C-C-C bond angles in the buckled carbon layer, instead of leading to significant out-of-plane fluctuations that occur in graphene.

RESULTS AND DISCUSSION

SYNTHESIS

Elias *et al*. reported the experimental fabrication of graphane in 2009. Graphene samples were extracted using micromechanical cleavage of graphite. These samples were either deposited on top of an oxidized Si substrate or used as free-standing membranes for transmission electron microscopy (TEM). The samples were first heated at high temperature to remove all possible contamination. Cold hydrogen plasma at pressure 0.1 mbar hydrogen-argon mixture (10% H_2) was used for 2 hours to expose graphene samples.

Raman spectroscopy is an effective tool to see the changes induced by hydrogenated graphene. Fig. 7 exhibits the evolution of Raman spectra for graphene, hydrogenated and annealed graphene samples. Hydrogenation also results in sharp *D* (1342 cm^{-1}) and *D*' (~1610 cm^{-1}) peaks and combination of both *D* + *D*' peak around 2950 cm^{-1} as compared with disordered and nanostructured carbon-based materials. The *D* peak in graphane appeared due to the breaking of the translational symmetry of the C-C sp^2 bonds after the formation of the C-H sp^3 bonds. The *D* peak for both side hydrogenated graphene is twice larger than single sided hydrogenated graphene, due to the formation of twice C-H bonds.

The metallic character of graphene from graphane can be recovered by annealing graphane in Ar atmosphere at 450ºC for 24 hours as shown in Fig. 7. Higher annealing temperature may damage the sample by introducing structural disorder which broaden the intensity of the bands indicating that the annealed graphene becomes hole-doped. All the defect related peaks (*D*, *D*', and *D* + *D*') were strongly suppressed.

Wojtaszek *et al*. created hydrogenated single and bi-layer graphene by an Ar-H_2 plasma produced in a reactive ion etching (RIE) system [49]. They showed that the chosen plasma conditions can prevent damage to the graphene sheet. The reported hydrogenation was 0.05% which can be further improved. The hydrogenation occurs due to the hydrogen ions from the plasma and not due to the fragmentation of water adsorbates on the graphene surface by highly accelerated plasma electrons.

Poh *et al*. studied the production of partially hydrogenated graphene using thermal exfoliation of graphite oxide in H_2 atmosphere under high pressure (60-150 bar) and temperature (200-500ºC) [50]. They found that a H_2 pressure of 100 bar at 500ºC was the most efficient reaction condition. This method does not require a plasma source in contrast to previous work and thus, a large amount of hydrogenated graphene can be produced [48].

Guisinger *et al*. used room temperature STM to investigate the atomic hydrogen passivation of dangling bonds at the interface between single layer graphene and silicon-terminated SiC which can strongly influence the electronic properties of the graphene overlayer. Since hydrogen did not diffuse through the graphene monolayer suggesting that the edge of graphene is chemically bound to the reconstructed SiC (0001) surface [51].

Luo *et al*. showed that the hydrogenation of graphene layers by hydrogen plasma is reversible, even at its saturated hydrogen coverage. The hydrogen coverage depends on various parameters such as plasma power and process duration. The hydrogenation rate of

graphene layers is controlled by the hydrogenation energy barriers, which show a clear dependence on the number of layers. It is demonstrated, using Raman spectroscopy, that the hydrogenation of bilayer and multilayer graphene is much more feasible than that of single layer graphene on SiO_2/Si substrate. The dehydrogenation also shows significant dependence on the numbers of graphene layers and the amount of hydrogen coverage [52].

Wang *et al*. reported a new route to prepare high quality, monolayer graphene by dehydrogenation of a graphane-like film grown by plasma-enhanced chemical vapor deposition. The advantage of the plasma deposition process is its compatibility with wafer scale processing and lithographical patterning as well as deposition on metal-coated silicon substrates at temperature at least 350ºC lower than that used in thermal CVD processes. Using laser writing, graphane-like ribbons and squares can be formed which is a step towards to design of an integrated circuit based on all-carbon electronics [53].

Jones *et al*. have synthesized partially hydrogenated graphene on both sides and on single side of graphene by electron irradiation of graphene having chemisorbed H_2O and NH_3 on the layer. Hydrogenation was proposed due to H^+ ions and H radicals resulting from the fragmentation of H_2O and NH_3 adsorbates by backscattered and secondary electrons [54].

Ryu *et al*. realized hydrogenation of graphene byelectron-induced dissociation of hydrogen silsesquioxane (HSQ). Hydrogenation occurred at a higher rate for single than for double layers due to the enhanced chemical reactivity of a single sheet of graphene. The probability of chemisorption of hydrogen atoms on single layers is at least 0.03 at room temperature which is 15 times large rthan for that for bilayers [55].

Theoretically, many authors proposed different approaches for the hydrogenation graphene.

Using density functional theory, Zhou *et al*. proposed semi-hydrogenated graphene by applying an external electric field to a fully hydrogenated graphene which can remove H atoms from one side of graphane [56-57]. Semi-hydrogenated graphene, also known as "graphone" is a ferromagnetic semiconductor with an indirect band gap of 0.43 eV. But it was shown that free-standing graphone will roll up [58]. In addition, Ao *et al*. showed that hydrogenation of graphene layers is easier when an electric field that acts as a catalis or for dissociative adsorption of H_2, is applied [61].

Leenaerts *et al*. performed ab initio density functional theory calculations to investigate the process of hydrogenation of a bilayer of graphene [62]. 50% hydrogen coverage is possible in case that the hydrogen atoms are allowed to adsorb on both sides of the bilayer. In this case, the weak vander Walls forces between the graphene layers are replaced by strong interlayer chemical bonds. At maximum coverage, a bilayer of graphane is formed which has similar electronic properties to those of a single layer of graphane due to the same hybridization. Such a bilayer can be viewed as the thinnest layer of diamond which was recently realized experimentally [63]. Samarakoon *et al*. studied the electronic properties of hydrogenated bilayer graphene by applying a perpendicular electric bias using DFT calculations which leads to a transition from semiconducting to metallic state [64]. Also, desorption of hydrogen from one layer in bilayer graphane yields a ferromagnetic semiconductor with a tunable band gap.

Balog *et al*. demonstrated that a bandgap can be opened in graphene by inducing patterned hydrogen chemisorption onto the Moire superlattice positions of graphene grown on an Ir (111) substrate [10]. Combined STM and ARPES results demonstrated that the observed hydrogen adsorbate structures were stable well above room temperature. The band gap was not very sensitive to the exact hydrogen adsorbate structure. These experimental results also support the concept of confinement-induced gap opening by periodic lattice perturbations. The gap was induced at the Fermi energy and was of sufficient size, such that it can be used for electronic applications at room temperature. Balog *et al*. presented STM studies to reveal the local adsorbate structure of atomic hydrogen on the basal plane of graphene on a SiC substrate [65]. Four types of configurations were formed by hydrogen pairs after exposing to a 1600 K D-atom beam. At low coverage the formation of hydrogen dimers occurred, while at higher coverage random adsorption into larger hydrogen clusters was observed. They also found that

the tunneling current of the STM tip can induce hydrogen desorption, which implies that the hydrogen atom is weakly bound to the graphene surface. The hydrogenation was reversible by annealing the substrate to 800ºC. The adsorption of atomic hydrogen onto the desired areas on the surface and to form nanopatterns via tip-induced desorption of hydrogen, opens the possibility of electronic and chemical functionalization of graphene surfaces via hydrogenation. Haberer *et al*. observed by angle-resolved photoemission spectroscopy that a gap can be opened up to 1.0 eV for a hydrogen coverage of 8% of graphene on Au [66].

ELECTRONIC PROPERTIES

The electronic property of a material is essential in device technology. Monolayer materials, with their reduced dimensionality, provide a suitable play-ground for the modification of the characteristic properties of materials at atomic scale. In order to control or modify the properties of graphane, which is a nonmagnetic semiconductor, one can suggest several techniques such formation of graphanes with different stoichiometry, creating various vacancies, doping with foreign atoms, application of strain and dimensional reduction.

(i) Graphanes with Various C/H Ratios

If the adsorption of H atoms is only allowed at one side of the graphene layer, some interesting theoretical materials can be formed. Hydrogenation of a single sublattice gives rise to a ferromagnetic material that was called graphone [56]. The stability of graphone is very weak because the H atoms try to form pairs [58, 67-68]. Its practical use is therefore rather questionable. In addition, some studies such as controlled H-domain formation on Ir (111) supported graphene, excitation-induced hydrogen dissociation from the graphane surface were already reported by experimental groups [59-60].

A more promising case of single-side adsorption is C_4H. This structure is built from H pairs in the very stable para configuration in which atoms are adsorbed on opposite C atoms in the graphene hexagons. When this structure is repeated, a 2×2 superstructure arises which is very stable in Fig. 8. In 2011, this 2D C_4H crystal was synthesized by Haberer et al. on a Au substrate [69]. Hydrogen plasmas were used to hydrogenate the graphene sample to a H/C ratio of 1:4. DFT calculations show that the resulting material contains an electronic band gap of 3.5 eV which is similar to graphane [69-70].

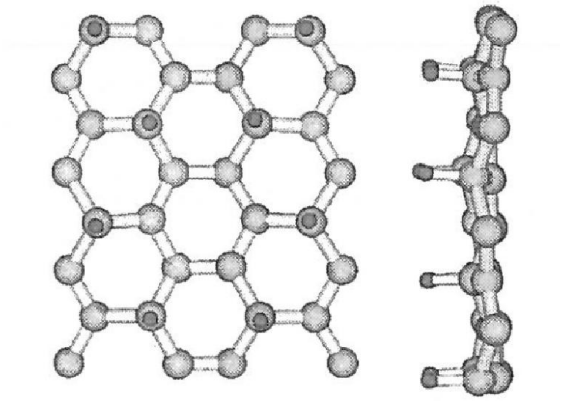

Fig. 8. Top and side view of the C_4H crystal structure.

It is also possible to hydrogenate multilayer graphene. This can be done in two different ways. First, the layers can all be completely hydrogenated to form stacked sequences of *e.g*. chair isomers, and second, only the top and bottom layer are hydrogenated from one side, resulting in a thin diamond films.

In addition, Fokin *et al*. studied the effect of σ-σ and π-π interactions in the electronic properties of single layer and multilayer [n] graphanes at the dispersion corrected density functional theory (DFT) level [71]. It was found that graphanes show quantum confinement effects as the HOMO-LUMO gaps decrease from small to large graphane structures, asymptotically approaching 5.4 eV previously obtained for bulk graphane. Similarly, Alonsoet *et al.* investigated the nature and origin of dispersion interactions for the benzene and cyclohexane dimers by using dispersion-corrected density functional theory, energy decomposition analysis, and the noncovalent interaction (NCI) method. Their NCI analysis revealed the dispersion interactions between the hydrogen atoms are responsible for the surprisingly strong aliphatic inter-actions.

Completely hydrogenated graphene layers can be stacked to form multilayered systems or 3*D* crystals.The H atoms of the different layers have a repulsive effect which causes the layers to align in such a way that the H atoms of one layer do not overlap with the H atoms of the neighboring graphane layer. The most stable multilayered graphane system is built from *AA*-stacked chair isomers [20, 73]. However, under pressure, other graphane configurations can become more favorable as building blocks for 3*D* graphane crystals. Wen *et al*. calculated that for pressures above 10 GPa, the stirrup isomer becomes more stable due to a more efficient interlayer H arrangement [20]. Pressure was also shown to increase the electronic band gap up to 20 GPa [20].

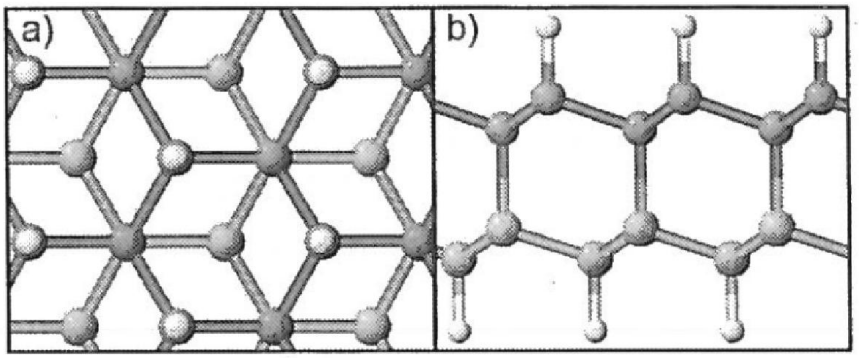

Fig. 9. Top and side view of bilayer diamane structure.

When the hydrogenation process of few-layer graphene (FLG) is restricted in such a way that only the outer layers are exposed to H atoms, it is possible to turn FLG in thin diamond films. Such films have been dubbed diamane. Hydrogen adsorption on the top layer changes the hybridization of the interacting C atoms to sp^3, but also the neighboring C atoms will undergo a substantial hybridization change [62]. When the H coverage is large enough, it becomes favorable for the non-hydrogenated C atoms in the outer layers to form covalent bonds with the underlying layers in Fig. 9. The formation of interlayer C-C bonds is easiest achieved in *AA* or *ABC*-stacked graphene layers, but has also been theoretically predicted for twisted graphene bilayers [74-77]. In addition, Mapasha *et. al*. investigated hydrogenation of bilayer graphene using *GGA-PBE* functional and four variants of non-local vander Waals density functionals *vdW-DF*, *vdW-DF*2, *vdW-DF-C*09*x* and *vdW-DF*2-*C*09*x* [78].

For ordered FLG slabs the process can be continued until all C atoms in the system have sp^3 hybridization. In this ways the hydrogenation process can turn FLG into a thin diamond film, as has been experimentally confirmed [63, 74-76]. The band gap of diamane decreases with the number of layers and does not converge to the band gap of bulk diamond [76, 79]. The reason for this is that the size of the band gap is determined by the position of the CBM which corresponds to a surface state in Fig. 4. As predicted by Samarakoon *et, al*., the band gap of bilayer diamane can also be tuned by the application of an electric field. The gap decreases monotonically with increasing field strength and a semiconductor to metal transition is observed at 1.05 V/Å [64].

(ii) Vacancy Formation

As it was shown before even the strong covalent bonds of graphene can be broken and various vacancies are formed due to *e.g*. continuous exposure to the high-energy electron beam or irradiation with low energy Ar^+ [80-81]. Moreover, the fabrication of large graphene sheets having a high-density of nanoscale holes or multiple carbon vacancies is another landmark in controlling the electronic properties of graphene [82-83].

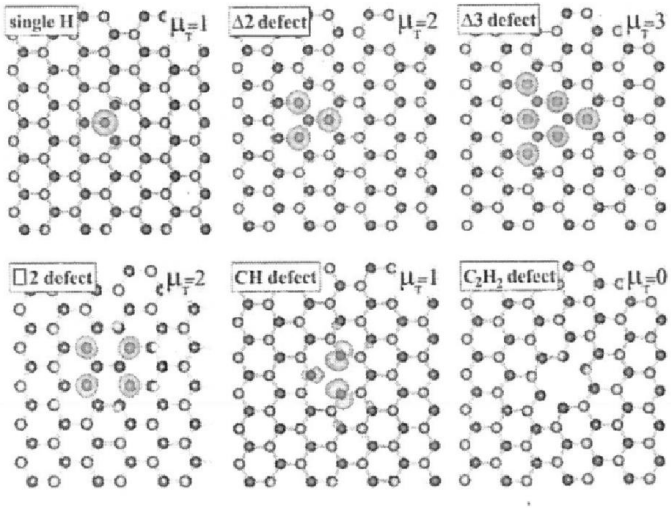

Fig. 10. Magnetic properties of graphane with various defects created by removing H atoms and C-H pairs

Therefore, motivated by these recent advances, controllable modification of the electronic properties of graphane, that has weaker covalent bonds as compared to graphene, can be utilized for different applications.

As was shown by Sahin *et. al*., desorption of a single H atom from the surface of graphane requires 4.79 eV energy per atom [33]. Formation of each H-vacancy leaves a half-filled sp^3 like orbital on the graphane surface and therefore the bandgap is reduced by the defect states that appear around the Fermi level. Here it is worth to note that each single H-vacancy creates a local magnetic moment of 1μB. As shown in Fig. 10, one can obtain large spin polarizations by creating triangular-shaped H-free regions on graphane. In addition, as long as the number of freed H atoms (C-H pairs) from A and B sublattice is the same there is no net magnetic moment in the ground state of the structure. Ferromagnetic domains with large net magnetic moments on graphane are useful for future data storage and spintronics applications. Likewise, Moaied *et, al.* reported that hydrogenation of single and multilayer graphene surfaces may result in a ferromagnetic state. It was also predicted that the Curie

temperature strongly depends on the size of the hydrogenated region. Similarly, a recent study by Walter *et. al.* showed that created vacancy domains on fluorographene, which is the fluorinated counterpart of graphane, possess a band gap which was reduced by midgap states resulting in a blue light emitting ground state which is not the case for defect-free material [86].

Creation of one-dimensional graphene/graphane superlattices with a tunable electronic bandgap can also be realized by selective desorption of H atoms. Hernandez-Nieves *et. al*. predicted, using *ab* initio calculations, that one-dimensional H-free regions serve as freestanding graphene nanoribbons, and their magnetic groundstate can be tuned via particular arrangements of the H atoms at the edges [87]. In recent work of Ray *et. al*., spintronics applications of the graphene supported graphone/graphane bilayer structure was investigated experimentally. It was shown that hydrogen plasma treatment of vertically aligned few layer graphene results in the formation of graphane/graphone layers with ferromagnetic ground state [88]. Therefore graphone/graphanebilayers with their hydrogen concentration dependent magnetic properties are promising for nanoscale spintronic device applications. It appears that the formation of H vacancies on graphane not only suitable for providing spin polarization but can also be used for the electronic characteristics.

(iii) Doping by Foreign Atoms

Although impurities such as single atoms, molecules and small clusters on ultra-thin materials appear as un-desirable residual from the synthesis process, these impurities can also be utilized for the modification of electronic and magnetic properties of these materials.

Lu *et. al*. showed that the electronic structure of fluorine doped graphane is very sensitive to the doping configuration, due to the competition between anti-bonding states and nearly surface states [89]. An interesting application of graphane, as a PNP transistor, was proposed by Gharekhanlou *et. al* [90]. Using graphane with hydrogen deficiency to reduce the band gap, it was shown that, within the approximation of the Shockley law for junctions, an exponential ideal I-V characteristic is expected and the curvature of the collector current characteristics shows good agreement with an ideal bipolar transistor.

Moreover, Hussain *et. al*. studied the stability and possibility of hydrogen storage applications of Ca-doped graphane. They found that Ca-doped graphane structure remains stable even at high temperatures and hydrogen storage capacity of a monolayer Ca-doped graphane with a doping concentration of 11% of Ca on a graphane sheet, and a reasonably good H_2 storage capacity of 6wt % could be attained [91]. In addition the same group reported that neither a pristine graphane sheet nor the sheet defected by removing a few surface H atoms have sufficient affinity for either H_2S or NH_3 gas molecules. However, a graphane sheet doped with Li add atoms shows a strong sensing affinity for both mentioned gas molecules [92].

Doping of graphane not only results in the modification of the electronic bandgap, but also can yield the emergence of novel phases in the material. Savini *et. al.* predicted by using first-principles calculations that p-doped graphane is an electron-phonon superconductor and the presence of a giant Kohn anomaly in the optical phonon dispersions, that originates from a large density of electronic states at the Fermi energy and strong carbon-carbon bonds, results in a superconducting phase [39]. In addition, using mean-field theory, Loktev *et. al*. considered superconducting properties of multilayer and single layer graphane by taking into account fluctuations of the order parameter [93].

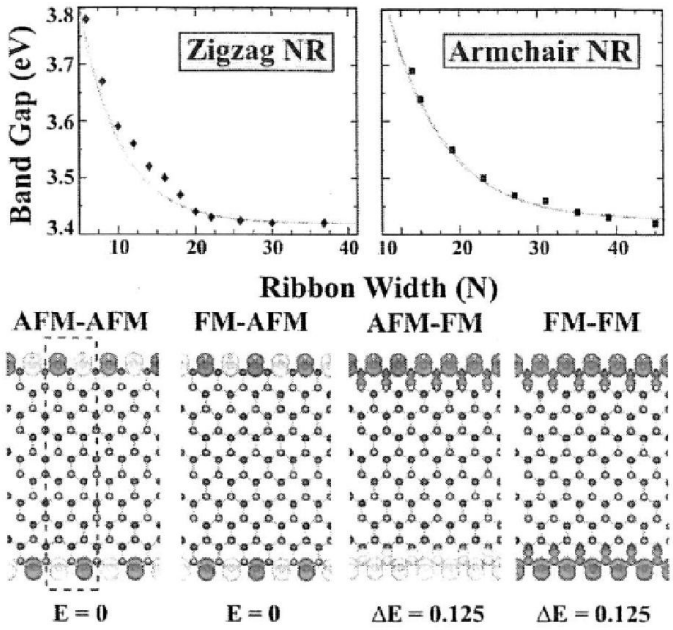

Fig. 11. Energy bandgap of zigzag and arm-chair nanoribbons as a function of ribbon width (Upper). Magnetic ground state analysis of zigzag graphane nanoribbons (Lower).

They showed that, even for low doping cases, in the single-layer and multilayer case the critical temperature is predicted to be 100 K and 150 K, respectively.

Da *et. al*. studied the magnetic properties of graphane by substituting the C atoms along with its attached H atoms with transition metal (TM) atoms [94]. It was also shown that a maximum magnetic moment of 3.5 μB can be reached by embedding Mn in graphane. In another DFT study by AlZahrani revealed that the hollow-site adsorption configuration on graphane is the most preferable one for Mn atoms [95]. Also, a heterojunction structure embedded with nickel and vanadium within graphane suppress the spin-down current while the spin-up current appears at the negative bias voltage, resulting in a spin current diode. Yang showed that creating a vacancy of a hydrogen atom generates a magnetic moment of 1μB and if this vacancy is occupied by transition metal elements, the magnetic moment can enhanced many fold [96]. Leenaerts *et. al.,* investigated the effect of substitutional doping of fluorographene with boron and nitrogen atoms on its electronic and magnetic properties using first-principles calculations. Boron dopants acted as shallow acceptors and caused hole doping but no changes in the magnetic properties were observed. Nitrogen dopants acted as deep donors and gave rise to a magnetic moment, but the resulting system became chemically unstable. These results are opposite to what was found for substitutional doping of graphane in which case *B* substituents induce magnetism and N dopants do not.

In addition, bandgap excitations graphane and its derivatives was studied by Nelson *et. al*. The nonradiative lifetime and radiative line width of the lowest energy singlet excitations in pure and oxidized graphanes were determined by performing non adiabatic molecular dynamics combined with time-dependent density functional theory [98].

(iv) Ribbons

Advances in experimental techniques have also made the synthesis of ultra-narrow one dimensional structures "few-atoms-wide ribbons" possible. Dimensional reduction of graphane is another efficient way of tuning its electronic properties. As reported by Sahin *et. al*. nanoribbons (NRs) of graphane have some distinctive properties [84]. It was shown that H-terminated armchair and zigzag graphane NRs display a band-gap reduction with increasing width in see Fig. 11. This behavior could be fitted to an expression $E_{gap} = 3.42 + \alpha escp(-N\beta)$ eV. Here α and β are fitting parameters and are found to be 1.18 (2.15) and 0.19 (0.14) for zigzag (armchair) graphane NRs. While bare zigzag graphane NR is an antiferromagnetic semiconductor with an indirect band gap relatively smaller than that of 2*D* graphane, armchair NRs are non-magnetic semiconductors. However, upon the saturation of edge atoms both NR, types become direct band-gap semiconductor having a nonmagnetic ground state.

Moreover, Zhang *et. al*., using the density functional theory methodology, predicted that the band gap of graphane nanoribbons can be tuned linearly with strain regardless of their widths or edge structures [99]. Moreover, the band gap of the graphane nanoribbon is more sensitive to compressive than tensile deformation, which mainly originates from the shift of its valence band edge under strain. In addition, another interesting property, the presence of two types of nearly-free-electron states in graphane NRs was predicted by Liu *et. al* [100]. It was also shown by Wu *et. al*. that by forming one-dimensional H-vacancy chains in graphane one can create various patterns of graphane/graphene NRs with tunable bandgaps [101, 87].

(v) STRAIN

Due to the atomic scale thickness of ultra-thin materials characteristic properties of them are quite sensitive to lattice deformations. As an efficient way, strain of two-dimensional materials has been widely studied to tailor the electronic properties of materials and improve their optical properties.

Elastic properties of graphane were first studied by Topsakal *et. al*., using DFT based strain energy calculations in the harmonic elastic deformation range [41]. It was found that graphane is a quite stiff material and although the applied strain has negligible effect on strong C-H bonds, stretched C-C bonds yield a dramatical modulation in the conduction band states in see Fig. 12.

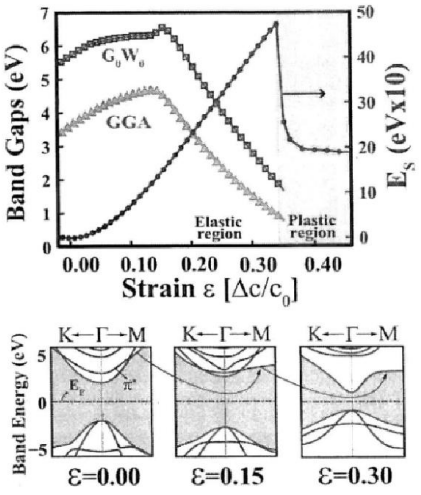

Fig. 12. Evolution of the energy bandgap (upper) and electronic dispersion (lower) as a function of strain

In addition, quantum-mechanochemical reaction coordinate simulations were performed by Popova *et. al*, to investigate the mechanical properties of graphane [102]. They showed that hydrogenation of graphene drastically influences the behavior and numerical characteristics of the body, making tricotage like pattern of graphene failureless pronounced and inverting. It from the zigzag to arm-chair mode as well as providing less mechanical resistance of graphane in total.

Recently, Pong *et. al*. studied the effect of dispersion forces on the mechanical properties of graphane [103]. By per-forming *DFT* calculations with *DFT-D*2 approximated vander Waals (vdW) corrections they showed that vdW has little effect on the geometry (< 0.4%) and the mechanical properties, including ultimate stresses (2%), ultimate strains (8.7%), in-plane stiffness (1%) and Poisson ratio (3%) .

Applications

As the demand for energy is increasing across the world and concerns over CO_2 emission to climate change, hydrogen has emerged as a potential candidate as energy carrier due to its combustion waste product water [104]. The advantage of using graphane as H_2 storage material is its nano-size, large stability and relatively stronger graphane-metal binding. Recently, Hussain *et. al*. showed that defected graphane functionalized both sides by poly-lithiated species CLi_3 and CLi_4, a storage capacity of more than 13 wt % can be achieved [92]. Further-more, the binding energies of the absorbed H_2 are in the range 0.25 eV-0.35 eV, which is well suited for an efficient H_2 storage. Hussain *et. al*. also studied the effect of strain on the adsorption of hydrogen on the lithium doped graphane system [91]. For strain-free case, at most 3 hydrogen molecules can be adsorbed on each Li resulting in a storage capacity of 9.37 wt%. While applying biaxial asymmetric strain, a stronger binding between Li-graphane occurs. Now at most 4 hydrogen molecules can be adsorbed on each Li enhancing the storage capacity to 12 wt% beyond the Department of Energy target of 2017. In addition, Xiao *et. al*. examined CO_2 adsorption over various N-substituted/grafted graphanes to identify the promotional effects of various N-functionalities have on the adsorption characteristics using *DFT*. It was found that the presence of co-adsorbed H_2O on the surface pro-motes CO_2 adsorption on both N- and NH_2-sites, with highly exothermic adsorption energies [105].

Frictionless, lubricant or near-frictionless surfaces may find applications in the various fields of materials science. Using the Prandtl-Tomlinson model together with ab initio calculations Cahangirov *et. al*. investigated the interlayer interaction under constant loading force and derived the critical stiffness required to avoid stick-slip behavior [107]. It was also shown that graphane and similar layered structures have low critical stiffness even under high loading forces due to their charged surfaces repelling each other. Similarly, Wang *et. al*. calculated the friction characteristics of graphane and fluorographene. Their calculations revealed the general mechanism of atomic-scale friction in various graphene-based layered materials where the interlayer interaction is dominated by vander Waals and electrostatic interactions.

Kim *et. al*. studied monolayer halogenated graphane using first-principles calculations [106]. Different configurations of hydrogen and halogen atoms (F, Cl, Br) attached to graphene break the inversion symmetry and hence give piezoelectricity. $(C_2HF)_n$ polar conformation was most energetically stable with piezoelectricity due to the change of the electron distribution around the F atoms. $(C_2HCl)_n$ showed an enhancement in the piezoelectricity but the stability was degraded.

Thermoelectric materials, that have gained importance in recent years, can be used for the development of new cooling and power generation methods. Using thermo-electric materials one can convert the thermal difference into electrical energy or use electrical current for the creation of temperature difference. For an efficient thermoelectric device good electrical conductivity and low thermal conductivity is essential. Considering these requirements Ni *et. al*. investigated the possible use of graphene as a thermoelectric device and predicted that disordered armchair graphane NRs are promising candidates for constructing thermoelectric materials [109]. The high figure of merit, low cost, and easy synthesis of graphane make it a viable choice for thermoelectric applications.

The detection of explosives is one of the main concern for a secure and safe society. Trinitrotoluene (TNT) which is the main component in explosives, is toxic to the environment and a possible source of cancer in humans. Recently, electrochemical methods have emerged due to its rapid response time, portability, accuracy and lower cost than other analytical methods. Seah *et. al*. used partially hydrogenated graphene and graphene as a sensing platform for TNT in seawater [110]. They found graphene is more sensitive due to large aromatic rings which favour surface accumulation or larger preconcentration of analytes. Moreover, Tan *et. al*. have demonstrated, using electrochemical methods, that graphane exhibits different electrochemical behavior towards oxidation/reduction of important biomarkers, such as ascorbic acid, dopamine and uric acid when compared to ordinary graphene [111].

Conclusions

In this paper we have discussed the so-called graphane from synthesis to applications. We have showed that one-by-one hydrogenation of graphene results in graphane which is a stable, direct bandgap insulator with strong C-H bonds. We also showed that for the synthesis of graphanes one can choose various methods such as hydrogen plasma exposure of graphene, thermal exfoliation of graphene oxides, STM assisted hydrogenation of graphene, plasma-enhanced CVD and electron-induced dissociation of HSQ on graphene. We have also presented that electronic and magnetic properties of graphene can be modulated by various techniques such as synthesis of graphanes with different C/H ratios, formation of vacancies, application of strain and dimensional reduction. Finally, we showed that hydrogenated graphenes may also found applications in various fields such as hydrogen storage, piezzo-electricity, thermo-electrics, explosive detection and biosensing devices. We believe that future studies on functionalized graphane will reveal many interesting properties of this material.

Acknowledgment

This work is supported by University Grants Commission, New Delhi (Grant No. PDFSS-2011-12-SC-UTT-2848), India. The authors are thankful to Prof. Jai Shanker, Department of Physics, Institute of Basic Science, Khandari Campus, Agra.

References

1. Chandra, S., *Acta Ciencia Indica*, **40**, 145 (2014).
2. Chandra, S., Rani, P., *Acta Ciencia Indica*, **41**, 207 (2015).
3. Novoselov, KS., Geim, A.K., Morozov, S.V., Jiang, D., Zang, Y., Dubonos, S.V., Grigorieva, I.V., Eirsov, A.A., *Science*, **306**, 666-669 (2004).
4. Novoselov, K.S., Geim, A.K., Morozov, S.V., Jiang, D., Katsnelson, M.I., Grigorievea, I.V., Dubonos, S.V., Firsov, A.A., *Nature*, **438**, 197-200 (2005).

5. Lee, C.G., Wei, X.D., Kysar, J.W., Hone, J., *Science*, **321**, 385-388 (2008).
6. Balandin, A.A., Ghosh, S., Bao, W., Calizo, I., Teweldebrhan, D., Miao, F., Lau, C.N., *Nano Lett*., **8**, 4283-4287 (2008).
7. Jung, I., Dikin, DA., Piner, R.D., Ruoff, R.S., *Nano Lett*., **8**, 902-907 (2008).
8. Jia-An, Y., Lede, X., Chou, MY., *Phys. Rev. Lett*., **103**, 086802 (2009).
9. Ezawa, M., *Nanomater and Nanotechnol*., **3**, 10 (2013).
10. Balog, R., Jorgensen, B., Nilsson, L., Andersen, M., Rienks, E., Bianchi, M., Fanetti, M., Laegsgaard, E., Baraldi, A., Lizzit, S., Sljivancanin, Z., Besenbacher, F., Hammer, B., Pedersen, TG., Hormann, P., Hornekaer, L., *Nat Mater*, **9**, 315319 (2010).
11. Rudorff, W.G., *Z. Anorg Allg Chem*., **253**, 281-296 (1947).
12. Ebert, L.B., Brauman, J.I., Huggins, R.A., *J Am. Chem. Soc*., **69**, 7841-7842 (1974).
13. Watancbe, N., Nakajima, T., Touhara, H., *Graphite fluorides*, Amsterdam, New York., Elsevier, (1988).
14. Charlier, J.C., Gonze, X., Michenaud, J.P., *Phys Rev*., **B 47**, 16162 (1993).
15. Sluiter, M.H.F., Kawazoe, Y., *Phys Rev*., **B 68**, 085410 (2003).
16. Sofo, J.O., Chaudhari, A.S., Barber, G.D., *Phys Rev*., **B 75**, 153401(2007) & *ACS Nano*., **3,** 4017-4022 (2009).
17. Samarakoon, D.K., Wang, X.Q., *ACS Nano*., **3**, 4017-4022 (2009).
18. Leenaerts, O., Peelaers, H., Hernandez-Nieves, A.D., Partoens, B., Peeters, F.M., *Phys Rev*., **B 82**, 8195436 (2010).
19. Artyukhov, V.I., Chernozationskii, L.A., *J. Phys. Chem.,* **A 114**, 5389-5396 (2010).
20. Wen, X.D., Hand, L., Labet, V., Tang, T., Hoffmann, T., Ashcroft, N.W., Oganov, A.R., Lyakhov, A.O., *Proc. Natl. Acad Sci*., **180,** 6833-6837 (2011).
21. Heyd, J., Scuseria, G.E., Ernzerhof, M., J. *Chem. Phys*., **118**, 8207-8215 (2003).
22. Heyd, J., Scuseria, G.E., Ernzerhof, M., *J. Chem. Phys*., **118**, 8207 (2003) & *J. Chem Phys*., **124**, 219906 (2006).
23. Paier, J., Marsman, M., Hummer, K., Kresse, G., *Chem. Phys.*, **124**, 154709 (2006).
24. Samarakoon, D.K., Chen, Z., Nicolas, C., Wang, X.Q., *Small*, **7**, 965-969 (2011).
25. Bhattacharya, A., Bhattacharya, S., Majumder, C., Das, G.P., *Phys Rev*., **B 83**, 033404 (2011)
26. He, C., Sun, L.Z., Zhang, C.X., Jiao, N., Zhang, K.W., Zhong, J., *Phys Status Solidi*, **RRL6**, 427-429 (2012).
27. Lebegue, S., Klintenberg, M., Eriksson, O., Katsnelson, M.I., *Phys Rev*., **B 79**, 245117 (2009).
28. Amini, M.N., Leenaerts, O., Partoens, B., Lamoen, D., *Phys Chem*., **C117**, 16242-16247 (2013).
29. Cudazzo, P., Attaccalite, C., Tokatly, I.V., Rubio, A., *Phys Rev. Lett*., **104**, 226804 (2010).
30. Huang, S., Liang, Y., Yang, L., *Phys Rev*., **B 88**, 075441 (2013).
31. Karlicky, F., Otyepka, M., *J. Chem. Theory Comput.*, **9**, 4155-4164 (2013).
32. Reshak, A.H., Auluck, S., *RSC Adv*., **4**, 37411-37418 (2014).
33. Sahin, H., Ataca, C., Ciraci, S., *Appl. Phys. Lett*., **95**, 222510 (2009).
34. Berashevic, J., Chakraborty, T., *Nanotechnology*, **21**, 355201 (2010).
35. Wan, Y., Ding, Y., Shi, S., Tang, W., *Apple Phys Lett*., **98**, 163104 (2011).
36. Castro Neto, AH., Guineam F., *Phys. Rev. Lett*., **103,** 026804 (2009).
37. Gmitra, M., Kochan, D., Fabian, J., *Phys Rev. Lett*., **110**, 246602 (2013).
38. Peelaers, H., Hernandez-Nieves, A.D., Leenaerts, O., Partoens, B., Peeters, F.M., *Appl Phys Lett.*, **98**, 051914-051916 (2011).
39. Savini, G., Ferrari, A.C., Giustino, F., *Phys Rev. Lett*., **105,** 037002 (2010).
40. Chechin, G.M., Dmitriev, S.V., Lobzenko, I.P., Ryabov, D.S., *Phy. Rev*., **B 90** (2014).
41. Topsakal, M., Cahangirov, S., Ciraci, S., *Appl. Phys Lett*., **96**, 091912-091915 (2010).
42. Munoz, E., Singh, A.K., Ribas, M.A., Penev, E.S., Yakobson, B.I., *Diam. Rel. Mat*., **19,**368-373 (2010).
43. Koenig, S.P., Boddeti, N.G., Dunn, M.L., Bunch, J.S., *Nat. Nanote*., **6**, 543-546(2010).
44. Nair, R.R., Ren, W., Jalil, R., Riaz, I., Kravets, V.G., Britnell, L., Blake, P., Schedin, F., Mayorov, A.S., Yuan, S., Katsnelson, M.I., Cheng, H.M., Strupinski, W., Bulusheva, L.G., Okotrub, A.V., Grigorieva, I.V., Grigorenko, A.N., Novoselov, K.S., Geim, A.K., *Small,* **6**, 2877-2884 (2010).
45. Colombo, L., Giordano, S., *Rep. Prog. Phys.,* **74**, 116501-116535 (2011).
46. Neek-Amal, M., Peeters, F.M., *Phys. Rev.,* **B83**, 235437 (2011).
47. Costamagna, S., Neek-Amal, M., Los, J.H., Peeters, F.M., *Phys. Rev.,* **B 86**, 041408 (2012).
48. Elias, D.C., Nair, R.R., Mohiuddin, T.M.G., Morozov, S.V., Blake, P., Halsall, M.P., Ferrari, A.C., Boukhvalov, D.W., Katsnelson, M.I., Geim, A.K., Novoselov, K.S., *Science*, **323**, 610-613 (2009).

49. Wojtaszek, M., Tombros, N., Caretta, A., van Loosdrecht, P.H.M., van Wees, B.J., *J. Appl. Phy*., **110,** 063715 (2011).
50. Poh, H.L., Sanek, F., Soferb, Z., Pumera, M., Nanoscale., **4**, 7006-7011 (2012).
51. Guisinger, N.P., Rutter, G.M., Crain, J.N., First, P.N., Stroscio, J.A., *Nano Lett*., **9**, 1462-1466 (2009).
52. Luo, ZQ., Yu, T., Kim, K.J., You, T.M., Lim, S., Shen, Z.X., *ACS Nano*., **3**, 1781-1788 (2009).
53. Wang, Y., Xu, X., Lu, J., Lin, M., Bao, Q., Ozyilmaz, B., Loh, K.P., *ACS Nano*., **4**, 6146-6152 (2010).
54. Jones, J.D., Mahajan, K.K., Williams, W.H., Ecton, P.A., Mo, Y., Perez, J.M., *Carbon.*, **48,** 2335-2340 (2010).
55. Ryu, S., Han, MY., Maultzsch, J., Heinz, T.F., Kim, P., Steigerwald, M.L., Brus, L.E., *Nano Lett*., **8**, 4597-4602 (2008).
56. Zhou, J., Wang, Q., Sun, Q., Chen, X.S., Kawazoc, Y., Jena, P., *Nano Lett*, **9**, 3867-3870 (2009).
57. Zhou, J., Wu, M.M., Zhou, X., Sun, Q., *Appl. Phys. Lett.,* **95**, 103108 (2009).
58. Neek-Amal, M., Beheshtian, J., Shayeganfar, F., Singh, S.K., Los, J.H., Peeters, F.M., *Phys. Rev.,* **B 87**, 075448 (2013).
59. Balog, R., Anderson, M., Jorgensen, B., Sljivancanin, Z., Hammer, B., Baraldi, A., *ACS Nano*., **7**, 3823 (2013).
60. Bang, J., Meng, S., Sun, Y.Y., West, D., Wang, Z.G., Gao, F., *Proc. Natl. Acad. Sci*., USA., **110**, 908 (2013).
61. Ao, Z.M., Peeters, F.M., *Appl. Phys. Lett*., **96**, 253106 (2010).
62. Leenaerts, O., Partoens, B., Peeters, F.M., *Phys. Rev.,* **B 88**, 245422 (2009).
63. Rajasekaran, S., Abild-Pedersen, F., Ogasawara, H., *Nilsson Phys Rev. Lett*., **111,** 085503 (2013).
64. Samarakoon, D.K., Wang, X.Q., *ACS Nano*., **4**, 4126-4130 (2010).
65. Balog, R., Jorgensem, B., Wells, J., Laegsgaard, E., Hofmann, P., Besenbacher, F., Hornekaer, L., *J. Am. Chem. Soc.,* **131,** 8744-8745 (2009).
66. Haberer, D., Vyalikh, D.V., Taioli, S., Dora, B., Farjam, M., Fink, J., Marchenko, D., Pichler, T., Ziegler, K., Simonucci, S., Dresselhaus, M.S., Knupfer, M., Buchner, B., Gruneis, A., *Nano Lett*., **10**, 3360-3366 (2010).
67. Podlivaev, A.I., Openov, L.A., *Semicond*, **45**, 958-961 (2011).
68. Pujari, B.S., Gusarov, S., Brett, M., Kovalenko, A., *Phys. Rev*., **B 84**, 041402 (2011).
69. Haberer, D., Guusca, C.E., Wang, Y., Sachdev, H., Fedrov, A.V., Farjam, M., Jafari, S.A., Vyalikh, D.V., Usachov, D., Liu, X.J., *Adv. Mater*., **23**, 4497-4503 (2011).
70. Li, Y., Chen, Z., *J. Phys. Chem.*, **C 116**, 4526-4534(2012).
71. Fokin, A.A., Gerbig, D., Schreiner, P.R., *J. Am. Chem. Soc.,* **133(50),** 20036-20039 (2011).
72. Alonso, M., Woller, T., Martin–Martinez, F.J., Contreras, Garcia J., Geerlings, P., De Proft, F., *Chem. Eur. J.,* **20**, 4931 (2014).
73. Rohrer, J., Hyldgaard, P., *Phys. Rev.,* **B 83,**165423 (2011).
74. Odkhuu, D., Shin, D., Ruoff, R.S, Park, N., *Scient Rep*,, **3**, 3276 (2013).
75. Kvashmin, A., Chernozatonskii, L.A., Yakobson, B.I., Sorokin, P.B., *Nano Lett.*, **14,**676-681 (2014).
76. Zhu, L., Hu, H., Chen, Q., Wang, S., Wang, J., Ding, F., *Nanotechnology*, **22**, 185202 (2011).
77. Muniz, A.R., Maroudas, D., *Phys. Rev.,* **B 86**, 075404 (2012).
78. Mapasha, R.E., Andrew, R.C., Chetty, N., *WIREs Comput. Mol. Sci*., **78,**1 (2013).
79. Chernozatondkii, L.A., Sorokin, P.B., Kuzubov, A.A., Sorokin, B.P., Kvashnin, A.G., Kvashmin, D.G., Avramov, P.V., Yakbson, B.I., *J. Phys. Chem.,* **C 115**, 132-136 (2011).
80. Kotakoski, J., Kraashenunnikov, A.V., Kaiserr, U., Meyer, J.C., *Phys, Rev, Lett*., **106,** 105505 (2011).
81. Ahlgren, E.H., Hamalainen, S.K., Lehtinen, O., Lijeroth, P., *Kotakoski J., Phys Rev*., **B 88**, 155419 (2013).
82. Bai, J., Zhong, X., Jiang, S., Huang, Y., Duan, X., *Nature Nanotech*, **5**, 190-194 (2010).
83. Lahiri, J., Lin, Y., Bozkurt, P., Oleynik, I.I., Batzill, M., *Nanotech*., **5**, 326-329 (2010).
84. Sahin, H., Atca, C., Ciraci, S., *Phys. Rev.,* **B 81**, 205417 (2010).
85. Moaied, M., Alvarez, J.V., Palacios, J.J., *Phys. Rev.,* **B 90**, 115441 (2014).
86. Walter, A.L., Sahin, H., Jeon, K.J., Bostwick, A., Horzum, S., Koch, R., Speck, F., Ostler, M., Nagel, P., Merz, M., Schupler, S., Schupler, S., Moreschini, L., Chang, Y.J., Seyller, T., Peeters, F.M., Horn, K., Rotemberg, E., *ACS Nano*, **8**, 7801-7808 (2014).
87. Hernandez-Nieves, A.D., Partoens, B., Peeters, F.M., *Phys. Rev.,* **B 82**, 165412 (2010).

88. Ray, S.C., Soin, N., Makgato, T., Chuang, C.H., Pong, W.F., Roy, S.S., Ghosh, S.K., Strydom, A.M., McLaughlin, J.A., *Sci. Rep.,* **4,**3862 (2014).
89. Lu, N., Li, Z., Yang, J., *J. Phys. Chem.,* **C 113**, 16741-16746 (2009).
90. Gharekhanlou, B., Tousaki, S.B., Khorasani, S., *J. Phys. Conf. Ser.,* **248**, 012061(2010).
91. Hussain, T., Pathak, B., Ramzan, M., Maark, TA., Ahuja, R., *Appl. Phys. Lett.,* **100,**183902 (2012).
92. Hussain, T., Panigrahi, P., Ahuja, R.. *Phys. Chem. Chem. Phys.,* **16,** 8100-8105 (2014).
93. Loktev, V.M., Turkowski, V., *J. Low Temp. Phys.,* **164**, 264-271 (2011).
94. Da, H., Feng, Y.P., Liang, G., *J. Phys. Chem.,* **C115**, 22701-22706 (2011).
95. AlZahrani, A.Z., *Phys.,* **B 407**, 992 (2012).
96. Yang, C.K., *Carbon*, **48**, 3901-3905 (2010).
97. Leenaerts, O., Sahin, H., Partoens, B., Peeters, F.M., *Phys. Rev.,* **B 88**, 035434 (2013).
98. Nelson, T.R., Prezhdo, O.V., *J. Am. Chem. Soc.,* **35**, 3702 (2013).
99. Zhang, Y., Wu, X., Li, Q., Yang, J., *J. Phys. Chem.,* **C 116**, 9356-9359 (2012).
100. Liu, Q.H., Li, Z.X.Y., Yang, J.L., Chin, *J. Chem. Phys.,* **24**, 22-24 (2011).
101. Wu, B.R., Yang, C.K., *AIP Advances*, **4,**087129 (2014).
102. Popova, N.A., Sheka, E.F., *J. Phys. Chem.,* **C 115**, 23745-23754 (2011).
103. Peng, Q., Chenb, Z., De, S., *Mech. Adv. Mater. Struc.,* **10**, 8339067 (2013).
104. Schlapbach, L., Ziittel, A., *Nature*, **414**, 353-358 (2001).
105. Xiao, J., Sitamraju, S., Janik, M.J., *Langmuir*., **30,** 1837 (2014).
106. Kim, H.J., Noor-A-Alam, M., Son, J.Y., Shin, Y.H., *Chem. Phys. Lett.,* **603**, 62-66 (2014).
107. Cahangirov, S., Atca, C., Topsakal, M., Sahin, H., Ciraci, S., *Phys. Rev. Lett.,* **108,** 126103 (2012).
108. Wang, L.F., Ma, T.B., Hu, Y.Z., Wang, H., Shao, T.M., *J. Phys. Chem.,* **C 117,** 12520 (2013).
109. Ni, X., Liang, G., Wang, J.S., Li, B., *Appl. Phys. Lett.,* **95,**192114 (2009).
110. Seah, T.H., Poh, H.L., Chua, C.K., Sofer, Z., Pumera, M., *Electroanalysis***, 26**, 62-68 (2014).
111. Tan, S.M., Sofer, Z., Pumera, M., *Electroanalysis,* **25**, 703-705 (2013).

❑